INTERNATIONAL JOURNAL OF HYDROGEN ENERGY XXX (2017) 1–8

Available online at www.sciencedirect.com

ScienceDirect

journal homepage: www.elsevier.com/locate/he

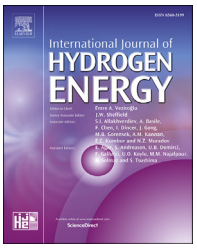

Versatile synthesis of molybdenum sulfide from confined spaces for efficient hydrogen evolution

Liao Chen [a], *Xiumei Geng* [a], *Lei Yang* [a], *Wentao Liang* [b], *Hongli Zhu* [a,*]

[a] *Department of Mechanical and Industrial Engineering, Northeastern University, Boston, MA 02115, USA*
[b] *Department of Biology, Northeastern University, Boston, MA 02115, USA*

ARTICLE INFO

Article history:
Received 28 July 2017
Received in revised form
13 September 2017
Accepted 19 September 2017
Available online xxx

Keywords:
Molybdenum sulfide
Confined growth
Hydrogen evolution reaction
Disulfide unit
Filler crystallite

ABSTRACT

(Quasi-)Amorphous molybdenum sulfide (MoS_x) materials with disulfide (S_2^{2-}) units have superior catalytic activities for hydrogen evolution reaction. However, the structures of the materials are less investigated and diversified. Herein, we first develop a new ethanol-thermal method to prepare MoS_x and further apply versatile confined growth treatment with low-cost filler crystallites to efficiently modify its structure and consequent performance. Expectedly, because the material is quasi-amorphous and very deformable, its morphology varies dramatically from granules to foam-like material with specific surface area increases from 22.53 m^2/g to 76.24 m^2/g under the restriction of confined spaces. Importantly, the amount of S_2^{2-} units which are responsible for the distinction of MoS_x increases as well. By virtue of the confined growth, the catalytic performance of the original material on hydrogen evolution is improved significantly. The over-potential required to obtain 10 mA cm^{-2} current decreases remarkably from 278 mV to 209 mV and the Tafel slope decreases from 160 mV/decade to 72 mV/decade after confined growth. Therefore, we have proposed an effective method to synthesize and promote the catalytic performance of MoS_x.

Introduction

Molybdenum sulfide materials have been recognized as promising non-precious hydrogen evolution reaction (HER) catalysts that are theoretically comparable to platinum. Among molybdenum sulfide catalysts, (quasi-)amorphous molybdenum sulfide (MoS_x) [1–6] exhibits superior activity to its high crystalline counterpart partially due to the boosting number of exposed active sites from the original inert basal plane [7–9] and the unique disulfide (S_2^{2-}) units [9–12] in MoS_x which are confirmed to be effective active sites for hydrogen evolution. Here, MoS_x is used to describe molybdenum sulfide materials which have slight or no crystallinity and also have characteristic S_2^{2-} units. By far, MoS_x materials are prepared by electrodeposition [13,14], photochemical reduction [15], thermolysis [11,16,17], and wet-chemical/hydro-thermal [3,18–21] methods. However, possibly due to the (quasi-)amorphous property, the structures of the materials are pretty simple and not enriched. Since structures of materials are critical to their performances, it is of good necessity to diversify the structures of the promising MoS_x materials.

In nature, the controllable formation of bio-minerals via amorphous materials in confined space is a principle utilized by organisms to produce tissues with sophisticated internal shapes and morphologies [22,23]. Thanks to the amorphous status without much anisotropy or preferred pattern, the precursors or final bio-minerals can be precisely molded into

* *Corresponding author.*
E-mail address: h.zhu@neu.edu (H. Zhu).

https://doi.org/10.1016/j.ijhydene.2017.09.106

enormous shapes easily. The complex amorphous bio-silica structure in diatom [24] and the aragonite tablets restricted by organic frames in the nacreous layer of mollusk shell [25] are typical examples of the principle. Though confined environments in templates have also been extensively used to prepare crystalline molybdenum disulfide (MoS_2) materials, the anisotropy of the crystalline materials may impede the continuous replication and full utilization of the confined spaces in sophisticated templates as implied by the poor spatial replication quality or non-continuous states of the final products [26–28]. However, researchers have replicated confined spaces in delicate biogenic and artificial structures successfully by virtue of deformable amorphous calcium carbonate which can penetrate deeply to form intimate contacts [29,30]. Now that the MoS_x materials also only have limited anisotropy and are highly deformable, intuitively, it is

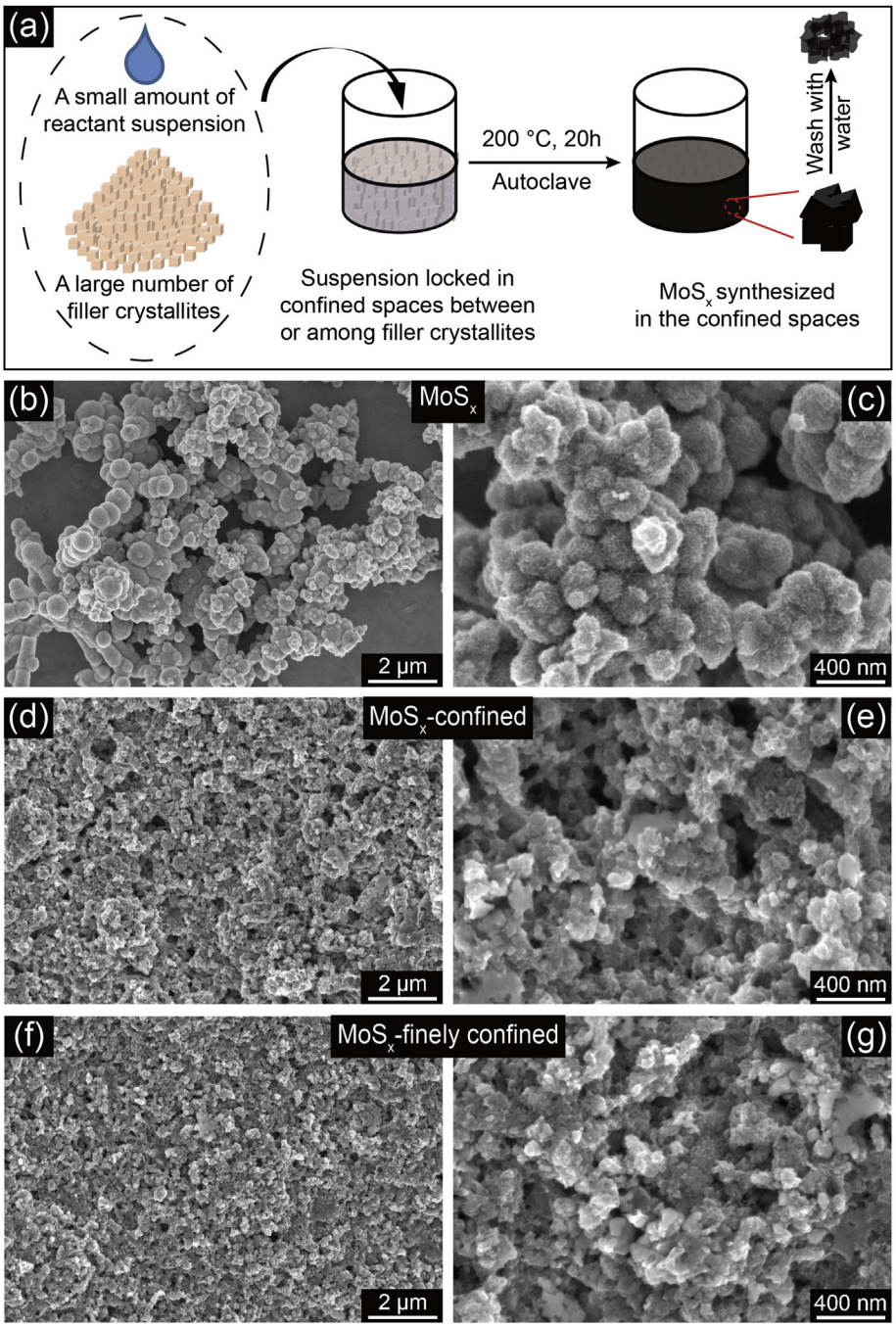

Fig. 1 – Morphologies of molybdenum sulfide (MoS_x) materials: (a) Schematic representation of the confined growth of MoS_x with filler crystallites; (b, c) SEM images of originally prepared unconfined MoS_x; (d, e) SEM images of MoS_x from confined growth; (f, g) SEM images of MoS_x from finely confined growth with grinded filler crystallites. The previous granular product will change its shape and become rather uniform after confined growth.

Please cite this article in press as: Chen L, et al., Versatile synthesis of molybdenum sulfide from confined spaces for efficient hydrogen evolution, International Journal of Hydrogen Energy (2017), https://doi.org/10.1016/j.ijhydene.2017.09.106

worth trying to apply confined growth principle to prepare those materials. Furthermore, confined conditions are known to influence the nucleation, growth and ultimately qualities of target materials [31–34]. Hence, it would be meaningful to modify and enrich the morphologies and structures of MoS_x materials with more active sites and consequently increasing efficiencies by confined growth.

Previously, graphene-protected 3D Ni foam [35], conductive graphene-carbon nanotube hybrids [36], and polystyrene particles were deposited with MoS_x [37] to produce catalysts for hydrogen evolution. Though the substrates/templates could improve the activity and possibly stability of MoS_x, the spaces in the substrates/templates were less confined and the preparation of the substrates/templates and/or the introduction of MoS_x were relatively complicated. Therefore, simple methods and inexpensive templates with readily available confined spaces that could be utilized to synthesize and regulate the MoS_x materials were highly desirable for the promotion of the promising MoS_x catalysts.

In this work, we first develop a new ethanol-thermal method to prepare MoS_x and then use ubiquitous sodium chloride as filler crystallites (Fig. S1) to create confined spaces to further regulate the growth of MoS_x (Fig. 1a). Two common reactants sodium molybdate dihydrate and thiourea are applied to grow MoS_x by ethanol-thermal method. Since sodium chloride filler crystallites do not dissolve in ethanol, a large number of filler crystallites are added to thoroughly disperse the tiny amount of reactants suspension, namely, the suspension exists only in the cavities between/among the filler crystallites. After reaction, the regulated MoS_x abound among the filler crystallites is harvested by dissolving the filler crystallites with water. Owing to the regulation of the confined spaces between/among filler crystallites, the morphology and performance of MoS_x alter markedly as expected with specific surface area increases ~3 folds, and the overpotential to reach 10 mA cm^{-2} current for hydrogen evolution decreases by 69 mV.

Results and discussion

The morphology of the as-prepared original MoS_x is mostly granular (Fig. 1b and c). However, when sodium chloride crystallites are introduced as filler crystallites to separate and lock the reaction suspension, MoS_x would grow between/among the filler crystallites and as a result of this, the

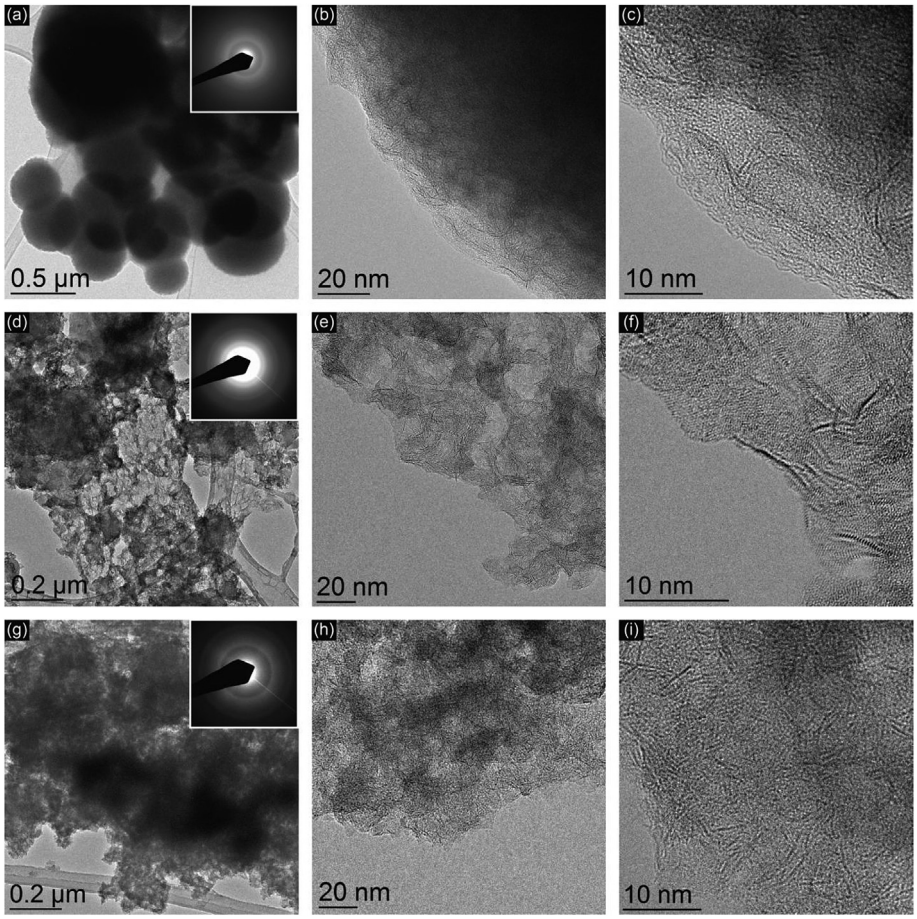

Fig. 2 – Transmission electron microscopy (TEM) images and selected area electron diffraction (SAED) patterns of MoS_x materials: (a–c) from originally unconfined growth; (d–f) from confined growth with regular filler crystallites; (g–i) from finely confined growth with grinded filler crystallites.

Please cite this article in press as: Chen L, et al., Versatile synthesis of molybdenum sulfide from confined spaces for efficient hydrogen evolution, International Journal of Hydrogen Energy (2017), https://doi.org/10.1016/j.ijhydene.2017.09.106

morphology of the final product is regulated by the confined spaces. The previous particle-like shape disappears and the obtained MoS_x shows a uniform structure (Fig. 1d and e). In order to further check the validity of the confined growth method, the as-bought sodium chloride crystallites are grinded into smaller particles (Fig. S1) to produce finer confined spaces for MoS_x growth. Predictably, the product become more uniform but with only slightly reduced feature size because the mortar-pestle-grinded filler crystallites are just a little smaller than the as-bought ones (Fig. 1f and g; Fig. S1). Accordingly, by confined growth with filler crystallites, the originally grown MoS_x can be modified successfully.

The poor crystallinities of the three types of products are indicated by selected area electron diffraction (SAED) in transmission electron microscopy (TEM). From TEM images, the originally grown MoS_x demonstrates granular morphology consisted of disorderly packed nano-sheets and/or atoms (Fig. 2a–c), whereas the two kinds of MoS_x from confined growth are foam-like materials formed by randomly packed nano-sheets and/or atoms (Fig. 2d–i). Because of the messy arrangement of the nano-sheets and/or atoms as implied by the scattered nano-sheet layers/fringes (Fig. 2 c, f, i), the SAED patterns of the three kinds of MoS_x materials are blurry broadened rings which indicate the poor crystallinity of the materials (Fig. 2a, d, g, insert). In addition, all the powder X-ray diffraction (PXRD) patterns further confirm that the materials are poorly crystalline (Fig. S2) and the pattern of the originally grown MoS_x (Fig. S2a) is even consistent with the reported patterns of amorphous molybdenum sulfide materials [18]. The two types of MoS_x grown from confined spaces have similar patterns which are different from that of originally grown MoS_x. Emerging peaks around 22° (Fig. S2b, c) of the two MoS_x materials from confined growth may be originated from the bundle-like assemblies of nano-sheets (Fig. 2e, f, h, i). Therefore, MoS_x of low crystallinity is synthesized and efficiently regulated by confined growth method.

The chemical states of molybdenum and sulfur are checked by X-ray photoelectron spectroscopy (XPS). The curves from the high resolution scans in Mo 3d and S 2p regions of the three types of MoS_x materials demonstrate similar features. All the three Mo 3d spectrums are deconvoluted into an S 2s peak and four Mo 3d peaks (Fig. 3 left; Table S1). The two Mo 3d peaks of the lowest and the third lowest binding energies can be assigned to Mo^{4+} centers in MoS_x. The peak at the second lowest binding energy may be attributed to Mo^{4+}/Mo^{5+} in MoS_xO_y while the one with the highest binding energy should be due to Mo^{6+} in MoO_3 which is possibly introduced by oxidation during sample preparation as also reported by others [3,36]. In addition, each characteristic broad S 2p spectrum can be best fitted with two doublets (Fig. 3 right; Table 1). The doublet at lower binding energy arises from basal

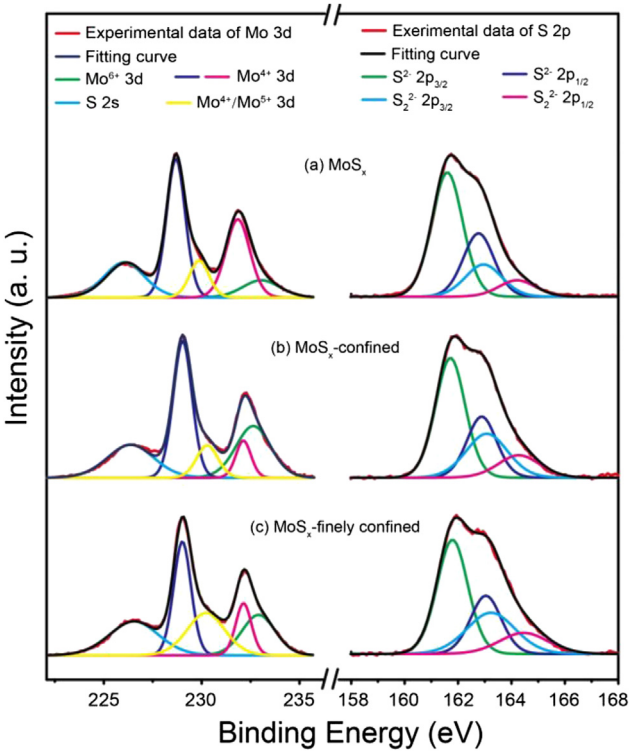

Fig. 3 – Deconvolution of XPS high resolution scans: Mo 3d (left) and S 2p (right) regions of (a) originally prepared MoS_x; (b) MoS_x from confined growth; (c) MoS_x from finely confined growth.

plane and apical S^{2-} while the doublet at higher binding energy is related with the existence of bridge and terminal S_2^{2-}. The Mo/S ratios and S_2^{2-} proportions quantified from XPS results are increasing after confined growth (Table 1). Accordingly, all the samples have the typical sulfur chemical states and the proportions of the S_2^{2-} units can be adjusted by confined growth.

Since the reactant suspensions and subsequent products are separated and locked by filler crystallites, it is natural to believe that the MoS_x materials grown from confined spaces will have increased specific surface areas. In fact, results of the nitrogen adsorption-desorption tests by the Brunauer–Emmett–Teller (BET) method are in evidence (Fig. 4a). The specific surface areas of the two types of MoS_x grown from confined spaces are 63.16 m^2/g and 76.24 m^2/g respectively while the value for originally grown MoS_x is only 22.53 m^2/g. Moreover, very possibly, the specific surface areas may reach even higher values by growing the material in finer and finer confined spaces. Besides the specific surface

Table 1 – Quantification of XPS data of MoS_x materials.

Samples	S^{2-} (eV)		S_2^{2-} (eV)		S_2^{2-} $2p_{3/2}/(S^{2-}+S_2^{2-})$	S_2^{2-} $2p_{1/2}/(S^{2-}+S_2^{2-})$	$S_2^{2-}/(S^{2-}+S_2^{2-})$	S/Mo
	$2p_{3/2}$	$2p_{1/2}$	$2p_{3/2}$	$2p_{1/2}$				
MoS_x	161.63	162.81	163.01	164.27	16.0%	8.5%	24.5%	2.48
MoS_x-confined	161.74	162.92	163.09	164.32	22.3%	11.4%	33.7%	2.71
MoS_x-finely confined	161.83	163.09	163.28	164.52	24.1%	12.2%	36.3%	2.75

Please cite this article in press as: Chen L, et al., Versatile synthesis of molybdenum sulfide from confined spaces for efficient hydrogen evolution, International Journal of Hydrogen Energy (2017), https://doi.org/10.1016/j.ijhydene.2017.09.106

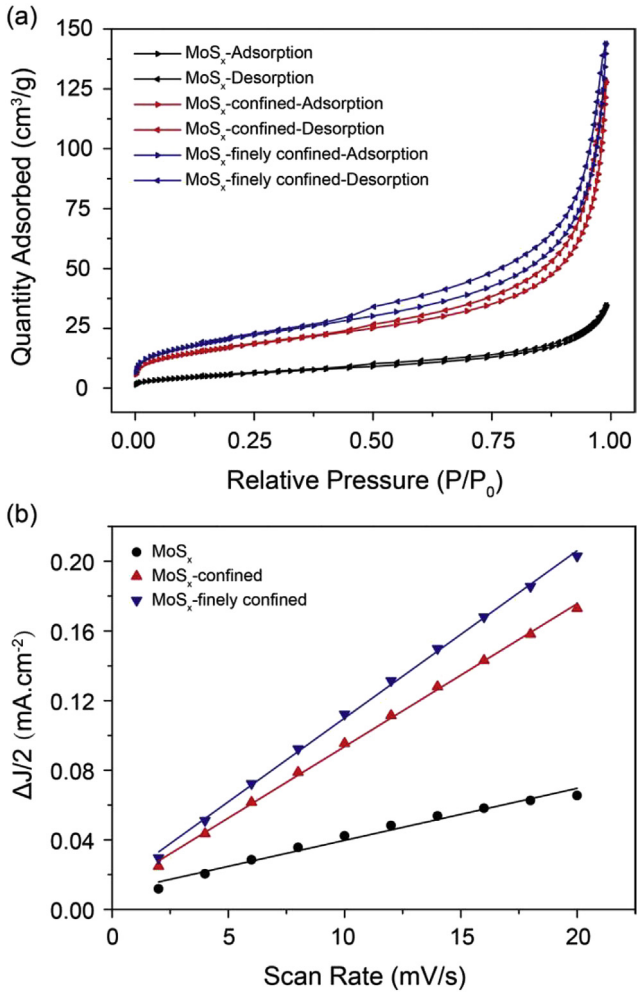

Fig. 4 – Surfaces areas of MoS_x materials: (a) Nitrogen adsorption–desorption isotherms of originally grown MoS_x (black line), MoS_x from confined growth with regular filler crystallites (red line) and from finely confined growth with grinded filler crystallites (blue line); (b) The double layer capacitances (directly proportional to effective electrochemical surface areas) of the three types of MoS_x materials. (For interpretation of the references to colour in this figure legend, the reader is referred to the web version of this article).

areas, effective electrochemical surface areas are measured by cyclic voltammograms (CVs) method [38–40]. Half values of the differences between the anodic and cathodic current densities (ΔJ/2) at the middle of CVs are plotted as a function of the scanning rate (Fig. 4b; Figure S4). By linear fitting, double layer capacitances obtained from the slopes of the fitting curves are 15.24, 41.78, 48.97 mF/cm^2 for original, confined and finely confined samples respectively. Because of the fact that double layer capacitances are directly proportional to effective electrochemical surface areas, the samples actually gain more effective electrochemical surface areas after confined growth which may also be responsible for the boosting performances. Hence, the MoS_x can accommodate and replicate the confined structures to some degree to expose more surface areas.

Without filler crystallites, during the reaction the nuclei come into being randomly and then atoms may assemble haphazardly into loosely packed nanosheets or aggregates to produce the granular MoS_x. When a large number of filler crystallites are used, the suspension liquid will only exists in the cavities between/among filler crystallites by osmotic pressure just like a tiny amount of water held by a lot of dry sand particles. Under the same reaction condition, the nucleation and the mass transportation will become rather difficult. Consequently, only reduced number of nuclei will form because of the high energy barrier and the nuclei may grow at a relatively low speed taking the impeded mass transportation into consideration [31–34]. Apparently, less nuclei and slow growth rate result in locally better packed materials but surrounded by a larger quantity of more randomly packed materials. Since the materials intrinsically tend to be amorphous, the improvements in crystalline qualities are limited and thanks to the poor crystallinities, the anisotropies of the materials are negligible and the materials do not grow into specific faceted shapes and will yield to the confinement of the filler crystallites. Due to the fact that the sizes of the confined spaces and the amount of locked suspension are limited, the MoS_x will sprawl among the confined spaces with restricted sizes. As a result, the granular product become foam-like materials with bulges after confined growth as revealed by TEM images (Fig. 2a, d, g). We suppose the foam-like morphology decorated with bulges may be caused by the growth in different kinds of confined spaces formed by filler crystallites, like the thin areas may grow from the confined spaces between two closely contact flat faces of filler crystallites while the bumps grow from spaces between rough surfaces or among obliquely aligned crystallites. In short, confined spaces can regulate the structures and also locally influence the qualities of the final products especially when the products are less crystalline.

Owing to the modified morphology and increased surface areas, it is expected that the MoS_x from confined growth will exhibit upgraded catalytic activities. The three types of MoS_x materials are applied to catalyze the hydrogen evolution reaction in 0.5 M sulfuric acid solution with a classical three-electrode setup. From the polarization curves, the two MoS_x catalysts modified by confined growth hold over-potentials at 10 mA cm^{-2} current of 215 mV and 209 mV respectively which are both remarkably lower than the corresponding 278 mV of their counterpart non-confined growth catalyst (Fig. 5a) and are also quite competitive among the performances of MoS_x materials prepared by the convenient wet-chemistry or solvothermal methods (Table 2). Tafel slopes are fitted according to the polarization curves and the also obvious discrepancies (160 mV/decade Vs. 72 or 76 mV/decade) support the distinction of the catalysts from confined growth (Fig. 5b). Moreover, the much smaller impedances of MoS_x materials from confined growth ensure their faster hydrogen evolution reaction kinetics (Fig. S5). The data of the three samples can be fitted with the same equivalent electric circuit (Fig. S5, inset). In the model, R_c and CPE_1 represent the contact between the glass carbon electrode and the catalyst, R_m stands for the electronic resistance of the catalyst, and R_{ct} is attributed to the charge transfer resistance [41]. Based on the fitting result, the R_{ct} seems mainly count for the differences between non-

Please cite this article in press as: Chen L, et al., Versatile synthesis of molybdenum sulfide from confined spaces for efficient hydrogen evolution, International Journal of Hydrogen Energy (2017), https://doi.org/10.1016/j.ijhydene.2017.09.106

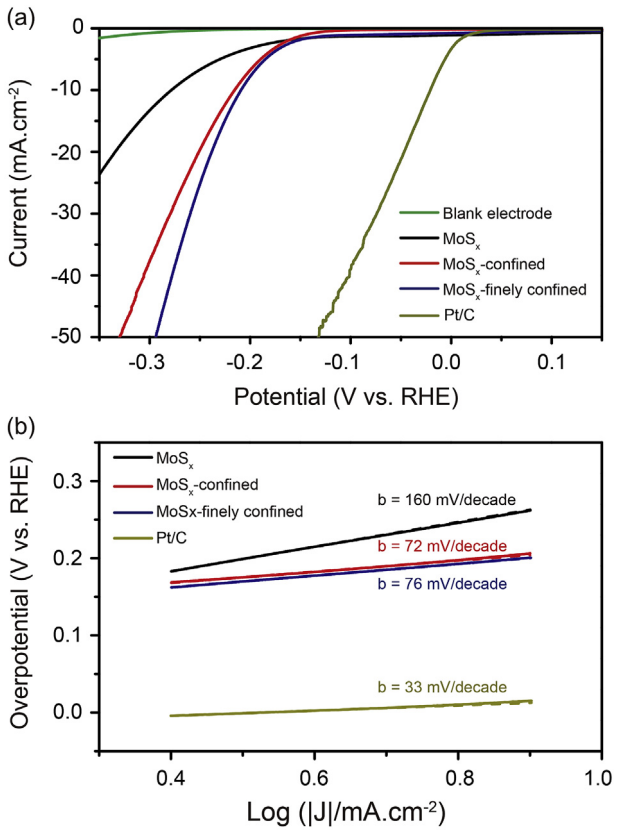

Fig. 5 – Hydrogen evolution reaction performance: (a) Polarization curves of the originally prepared MoS_x, confined and finely confined MoS_x, (b) Tafel plots of the three types of materials and the dash lines are the corresponding linear fitting of the plots.

Table 2 – HER performances of typical MoS_x materials prepared by wet-chemistry or solvothermal methods.

Samples	Over-potential to achieve 10 mA cm^{-2} current (mV)	Tafel slope (mV/decade)	Ref
MoS_x from confined growth	209–215	72–76	This work
Wet-chemical-synthesized MoS_x	198–204	53 to 65	Ref. [3]
Carbon-based MoS_x	202–225	50–78	Ref. [20]
MoS_3/multi-walled carbon nanotubes	210–225	40–57	Ref. [21]
$MoS_{2.7}$ @ nanoporous gold	~220	41	Ref. [27]
MoS_x grown with/without polystyrene particles	202–245	48–87	Ref. [37]
MoS_x on pretreated carbon fiber paper	205–231	46–50	Ref. [39]

confined and confined samples (Table S2). Since disulfide (S_2^{2-}) units are proved to be active sites in MoS_x materials [9–12], the increasing proportions of disulfide units (Table 1) after confined growth calculated from XPS data may contribute to the outstanding performances of confined growth samples. Actually, direct post-thermal-treatment to anneal the as-prepared MoS_x together with regular filler crystallites will weaken the catalytic activities of materials (Fig. S6) possibly due to the decreasing S_2^{2-} units and/or increasing crystallinities [9,42]. Besides, the nanosheets morphology together with extra defects from the quasi-amorphous basal plane and the tripled specific and effective electrochemical surface areas are beneficial as well. Though MoS_x catalysts are recognized as having more active sites, they are less stable than the corresponding catalysts with high crystallinities [2,9,36]. Here, the stabilities of the three samples are checked and the performances after 100 cycles decreases similarly and reasonably (Fig. S7). The sparse crystalline domains in the material might pin and stabilize a certain range of material in the catalyst. Consequently, the catalytic performance of originally prepared MoS_x can be considerably enhanced by confined growth.

Conclusion

In summary, MoS_x is synthesized by a convenient ethanol-thermal method and the originally obtained MoS_x of low crystallinity and with characteristic S_2^{2-} units can be effectively modified by confined growth. The morphology will change dramatically from granular particles to uniform structures after growing in the confined spaces constructed by stacked cheap filler crystallites. As the specific surface area, effective electrochemical surface area and the proportion of active disulfide (S_2^{2-}) units increase, the confined growth MoS_x possesses significantly promoted catalytic activity for hydrogen evolution reaction and the performance may be further improved by using even finer confined spaces. The overpotential at 10 mA cm^{-2} current decreases from 278 mV to 215 mV and then to 209 mV by confined growth with regular and grinded filler crystallites. Therefore, this work provides an efficient ethanol-thermal method together with confined growth to prepare MoS_x materials of remarkably promoted qualities and the confined growth strategy may potentially be applied to enhance the performances of other (quasi-)amorphous materials.

Experiment

Synthesis of MoS_x materials

In a typical procedure, 40 mg sodium molybdate (Sigma ≥99.5%) and 60 mg thiourea (Sigma ≥99.0%) were dispersed in 10 mL ethanol by stirring for 1 h. Then the suspension was put into a 25 mL autoclave reactor and the reactor was placed in a 200 °C oven for 20 h. After reaction, the auto clave reactor was taken out and put in ambient condition to cool down naturally. The black dispersive MoS_x product was obtained and washed by deionized water for at least 3 times.

For confined and finely confined growth, the same recipe as above was used and after the 10 mL reactant suspension being transferred into the autoclave reactor, about 20 mL sodium chloride filler crystallites (Morton Salt, as-bought or

Please cite this article in press as: Chen L, et al., Versatile synthesis of molybdenum sulfide from confined spaces for efficient hydrogen evolution, International Journal of Hydrogen Energy (2017), https://doi.org/10.1016/j.ijhydene.2017.09.106

grinded) were added into the reactor slowly with agitation. The reactor was placed still for 5 min and then the supernatant liquid was removed, namely the liquid existed only between/among the filler crystallites. In the cases of other filler/suspension ratios, the same procedures were complied with. Under 200 °C for 20 h, the as-grown MoS_x would fill all the confined spaces formed by filler crystallites. The filler crystallites were dissolved by water to collect the products and the obtained products were washed by deionized water for at least 6 times.

Direct post-thermal-treatment was utilized to anneal the as-prepared MoS_x materials while maintaining the structures from confined growth. In the above procedures, reaction took place at 200 °C for 20 h. Here, after the preparation of MoS_x materials, another 24 h or 48 h at 200 °C or 48 h at 220 °C were applied to post-thermal-treat confined MoS_x materials with regular filler crystallites directly in the autoclave reactor. After the post-thermal-treatment, the filler crystallites were dissolved and the products were washed as above.

Materials characterization

The morphologies of the materials were imaged by scanning electron microscopy (SEM, Hitachi SL4800) at 3 KV and by high resolution transmission electron microscopy (JEOL 2010F). Selected area electron diffraction (SAED) patterns were conducted on the same TEM. Crystallinity information was also collected from powder X-ray diffraction (PANalytical/Philips X'Pert Pro) with Cu (K_α radiation, $\lambda = 1.540598$ Å) as the anode material. The data is collected from 2θ of 5° to 80° with a scan rate of 1°/min. Specific surface areas of the materials were calculated by Brunauer–Emmett–Teller (BET) method after measuring the nitrogen adsorption-desorption isotherms at 77.3 K with Tristar II 3020 instrument. X-ray photoelectron spectroscopy (XPS) spectrum was obtained on Thermo Scientific K-Alpha XPS system equipped with a monochromatic soft Al Kα X-ray source ($h\nu = 1.4866$ keV, line width at ~0.3 eV). For the fitting of XPS curves in Mo 3d and S 2p regions, the peak area ratio of each doublet is determined by the degeneracy of the spin state. The binding energy separation of doublet between S $2p_{3/2}$ and S $2p_{1/2}$ is 1.2 ± 0.1 eV.

Electrochemical measurements

A classical three-electrode setup with glassy carbon as working electrode, platinum plate as counter electrode and saturated calomel electrode (SCE) as reference electrode was used for all the measurements. The SCE reference electrode was calibrated with comparison to reversible hydrogen electrode (RHE). The calibration was conducted in H_2 saturated electrolyte with Pt wire as the working electrode. In 0.5 M H_2SO_4, E(RHE) = E(SCE) + 0.289 V and all the potentials in our manuscript were corresponding to RHE.

The three types of MoS_x catalysts (original, confined and finely confined) were dispersed in mixed solvents (V_{H2O}: $V_{Ethanol}$ = 4:1) to prepare solutions of 1.32 mg/mL catalyst. Then, 20 μL of each suspension was dropped onto glassy carbon electrode of 5 mm in diameter and dried for 24 h. Linear sweep voltammetry was tested on a Biologic potentiostat at a scan rate of 3 mV/s in 0.5 M sulfuric acid solution. Electrochemical impedance was carried out at over-potential of 0.20 V in a range of 1×10^6 Hz–0.01 Hz under a voltage of 10 mV. For determination of the double layer capacitances by cyclic voltammograms (CVs) method, the CVs were measured under different scanning rates (2, 4, 6, 8, 10, 12, 14, 16, 18, 20 mV/s) within a potential range of 0.335–0.435 V vs. RHE where no faradic current was presented.

Acknowledgement

H. L. Zhu acknowledges the financial startup support and Tier 1 award from Northeastern University. We also thank George J. Kostas Nanoscale Technology and Manufacturing Research Center in Northeastern University and Center for Nanoscale System in Harvard University for using their facilities. We thank Dr. Xiulei Ji in Oregon State University for helping the BET test.

Appendix A. Supplementary data

Supplementary data related to this article can be found at https://doi.org/10.1016/j.ijhydene.2017.09.106.

REFERENCES

[1] Merki D, Fierro S, Vrubel H, Hu XL. Amorphous molybdenum sulfide films as catalysts for electrochemical hydrogen production in water. Chem Sci 2011;2:1262–7.
[2] Morales-Guio CG, Hu XL. Amorphous molybdenum sulfides as hydrogen evolution catalysts. Acc Chem Res 2014;47:2671–81.
[3] Benck JD, Chen ZB, Kuritzky LY, Forman AJ, Jaramillo TF. Amorphous molybdenum sulfide catalysts for electrochemical hydrogen production: insights into the origin of their catalytic activity. ACS Catal 2012;2:1916–23.
[4] Lee SC, Benck JD, Tsai C, Park J, Koh AL, Abild-Pedersen F, et al. Chemical and phase evolution of amorphous molybdenum sulfide catalysts for electrochemical hydrogen production. ACS Nano 2016;10:624–32.
[5] Tran PD, Tran TV, Orio M, Torelli S, Truong QD, Nayuki K, et al. Coordination polymer structure and revisited hydrogen evolution catalytic mechanism for amorphous molybdenum sulfide. Nat Mater 2016;15:640–6.
[6] Deng YL, Ting LRL, Neo PHL, Zhang YJ, Peterson AA, Yeo BS. Operando raman spectroscopy of amorphous molybdenum sulfide (MoS_x) during the electrochemical hydrogen evolution reaction: identification of sulfur atoms as catalytically active sites for H^+ reduction. ACS Catal 2016;6:7790–8.
[7] Xie JF, Xie Y. Structural engineering of electrocatalysts for the hydrogen evolution reaction: order or disorder? Chemcatchem 2015;7:2568–80.
[8] Nguyen DN, Nguyen LN, Nguyen PD, Thu TV, Nguyen AD, Tran PD. Crystallization of amorphous molybdenum sulfide induced by electron or laser beam and its effect on H_2 evolving activities. J Phys Chem C 2016;50:28789–94.
[9] Li YP, Yu YF, Huang YF, Nielsen RA, Goddard WA, Li Y, et al. Engineering the composition and crystallinity of molybdenum sulfide for high-performance electrocatalytic hydrogen evolution. ACS Catal 2015;5:448–55.

[10] Ting LRL, Deng YL, Ma L, Zhang YJ, Peterson AA, Yeo BS. Catalytic activities of sulfur atoms in amorphous molybdenum sulfide for the electrochemical hydrogen evolution reaction. ACS Catal 2016;6:861–7.
[11] Hsu CL, Chang YH, Chen TY, Tseng CC, Wei KH, Li LJ. Enhancing the electrocatalytic water splitting efficiency for amorphous MoSx. Int J Hydrogen Energy 2014;39:4788–93.
[12] Lassalle-Kaiser B, Merki D, Vrubel H, Gul S, Yachandra VK, Hu XL, et al. Evidence from in situ X-ray absorption spectroscopy for the involvement of terminal disulfide in the reduction of protons by an amorphous molybdenum sulfide electrocatalyst. J Am Chem Soc 2015;137:314–21.
[13] Vrubel H, Hu XL. Growth and activation of an amorphous molybdenum sulfide hydrogen evolving catalyst. ACS Catal 2013;3:2002–11.
[14] Belanger D, Laperriere G, Marsan B. The electrodeposition of amorphous molybdenum sulfide. J Electroanal Chem 1993;347:165–83.
[15] Hou J, Lei Y, Wang F, Ma X, Min S, Jin Z, et al. In-situ photochemical fabrication of transition metal promoted amorphous molybdenum sulfide catalysts for enhanced photosensitized hydrogen evolution. Int J Hydrogen Energy 2017;42:11118–29.
[16] Zhang T, Kong LB, Dai YH, Yan K, Shi M, Liu MC, et al. A facile strategy for the preparation of MoS_3 and its application as a negative electrode for supercapacitors. Chem Asian J 2016;11:2392–8.
[17] Liang KS, Cramer SP, Johnston DC, Chang CH, Jacobson AJ, Deneufville JP, et al. Amorphous MoS_3 and WS_3. J Non-Cryst Solids 1980;42:345–56.
[18] Nagaraju G, Tharamani CN, Chandrappa GT, Livage J. Hydrothermal synthesis of amorphous MoS_2 nanofiber bundles via acidification of ammonium heptamolybdate tetrahydrate. Nanoscale Res Lett 2007;2:461–8.
[19] Guo M, Wu Q, Yu M, Wang Y, Li M. One-step liquid phase chemical method to prepare carbon based amorphous molybdenum sulfides: as the effective hydrogen evolution reaction catalysts. Electrochim Acta 2017;236:280–7.
[20] Weber T, Muijsers JC, Niemantsverdriet JW. Structure of amorphous MoS_3. J Phys Chem US 1995;99:9194–200.
[21] Lin TW, Liu CJ, Lin JY. Facile synthesis of MoS3/carbon nanotube nanocomposite with high catalytic activity toward hydrogen evolution reaction. Appl Catal B Environ 2013;134:75–82.
[22] Hildebrand M. Diatoms, biomineralization processes, and genomics. Chem Rev 2008;108:4855–74.
[23] Sommerdijk NAJM, Colfen H. Lessons from nature-biomimetic approaches to minerals with complex structures. MRS Bull 2010;35:116–21.
[24] Sumper M, Kroger N. Silica formation in diatoms: the function of long-chain polyamines and silaffins. J Mater Chem 2004;14:2059–65.
[25] Addadi L, Joester D, Nudelman F, Weiner S. Mollusk shell formation: a source of new concepts for understanding biomineralization processes. Chem Eur J 2006;12:981–7.
[26] Kibsgaard J, Chen ZB, Reinecke BN, Jaramillo TF. Engineering the surface structure of MoS_2 to preferentially expose active edge sites for electrocatalysis. Nat Mater 2012;11:963–9.
[27] Ge XB, Chen LY, Zhang L, Wen YR, Hirata A, Chen MW. Nanoporous metal enhanced catalytic activities of amorphous molybdenum sulfide for high-efficiency hydrogen production. Adv Mater 2014;26:3100–4.
[28] Wang Y, Wang SS, Li CY, Qian M, Bu J, Wang JX, et al. Facile growth of well-dispersed and ultra-small MoS_2 nanodots in ordered mesoporous silica nanoparticles. Chem Commun 2016;52:10217–20.
[29] Finnemore AS, Scherer MRJ, Langford R, Mahajan S, Ludwigs S, Meldrum FC, et al. Nanostructured calcite single crystals with gyroid morphologies. Adv Mater 2009;21:3928–32.
[30] Li C, Qi LM. Bioinspired fabrication of 3D ordered macroporous single crystals of calcite from a transient amorphous phase. Angew Chem Int Ed 2008;47:2388–93.
[31] Asenath-Smith E, Li HY, Keene EC, Seh ZW, Estroff LA. Crystal growth of calcium carbonate in hydrogels as a model of biomineralization. Adv Funct Mater 2012;22:2891–914.
[32] Chernov AA. Modern crystallography III: crystal growth. New York: Springer-Verlag; 1984.
[33] Henisch HK. Crystals in gels and liesegang rings. New York: Cambridge University Press; 1988.
[34] Kliya MO, Sokolova IG. The question of the growth of crystals in porous media. Sov Phys Crystallogr 1958:487–93.
[35] Chang YH, Lin CT, Chen TY, Hsu CL, Lee YH, Zhang WJ, et al. Highly efficient electrocatalytic hydrogen production by MoS_x grown on graphene-protected 3D Ni foams. Adv Mater 2013;25:756–60.
[36] Pham KC, Chang YH, McPhail DS, Mattevi C, Wee ATS, Chua DHC. Amorphous molybdenum sulfide on graphene-carbon nanotube hybrids as highly active hydrogen evolution reaction catalysts. ACS Appl Mater Inter 2016;8:5961–71.
[37] Ambrosi A, Pumera M. Templated electrochemical fabrication of hollow molybdenum sulfide microstructures and nanostructures with catalytic properties for hydrogen production. Acs Catal 2016;6:3985–93.
[38] Wang HT, Lu ZY, Kong DS, Sun J, Hymel TM, Cui Y. Electrochemical tuning of MoS_2 nanoparticles on three-dimensional substrate for efficient hydrogen evolution. ACS Nano 2014;8:4940–7.
[39] Bose R, Balasingam SK, Shin S, Jin Z, Kwon DH, Jun Y, et al. Importance of hydrophilic pretreatment in the hydrothermal growth of amorphous molybdenum sulfide for hydrogen evolution catalysis. Langmuir 2015;31:5220–7.
[40] Lu AY, Yang XL, Tseng CC, Min SX, Lin SH, Hsu CL, et al. High-sulfur-vacancy amorphous molybdenum sulfide as a high current electrocatalyst in hydrogen evolution. Small 2016;12:5530–7.
[41] Vrubel H, Moehl T, Gratzel M, Hu XL. Revealing and accelerating slow electron transport in amorphous molybdenum sulphide particles for hydrogen evolution reaction. Chem Commun 2013;49:8985–7.
[42] Ratnasamy P, Rodrique L, Leonard AJ. Structural and textural studies in molybdenum sulfide systems. J Phys Chem 1973;77:2242–5.

Please cite this article in press as: Chen L, et al., Versatile synthesis of molybdenum sulfide from confined spaces for efficient hydrogen evolution, International Journal of Hydrogen Energy (2017), https://doi.org/10.1016/j.ijhydene.2017.09.106